

Direct observation of the quantum critical point in heavy fermion CeRhSi₃

N. Egetenmeyer,^{1,*} J. L. Gavilano,¹ A. Maisuradze,^{2,3} S. Gerber,¹ M. Kenzelmann,⁴ G. Seyfarth,⁵ D. Andreica,⁶ A. Desilets-Benoit,⁷ A. D. Bianchi,⁷ Ch. Baines,² R. Khasanov,² and D. E. MacLaughlin⁸

¹Laboratory for Neutron Scattering, Paul Scherrer Institut, CH-5232 Villigen PSI, Switzerland

²Laboratory for Muon Spin Spectroscopy, Paul Scherrer Institut, CH-5232 Villigen PSI, Switzerland

³Physik-Institut der Universität Zürich, Winterthurerstrasse 190, CH-8057 Zürich, Switzerland

⁴Laboratory for Developments and Methods, Paul Scherrer Institut, CH-5232 Villigen PSI, Switzerland

⁵DPMC, Université de Genève, CH-1211 Geneva, Switzerland

⁶Faculty of Physics, Babes-Bolyai University, RO-400084 Cluj-Napoca, Romania

⁷Département de Physique, Université de Montréal, Montréal H3C 3J7, Canada

⁸Department of Physics and Astronomy, University of California, Riverside, California 92521, USA

(Dated: February 7, 2012)

We report on muon spin rotation (μ SR) studies of the noncentrosymmetric heavy fermion antiferromagnet CeRhSi₃. A drastic and monotonic suppression of the internal fields, at the lowest measured temperature, was observed upon increase of external pressure. Our data suggest that the ordered moments are gradually quenched with increasing pressure, in a manner different from the pressure dependence of the Néel temperature. At 23.6 kbar the ordered magnetic moments are fully suppressed via a second order phase transition and T_N is zero. Thus, we directly observed the quantum critical point at 23.6 kbar hidden inside the superconducting phase of CeRhSi₃.

PACS numbers: 76.75.+i, 75.50.Ee, 75.30.Mb, 75.40.Cx

The role of magnetism in many superconducting materials is a topic of intense research. Often, these materials display a quantum critical point (QCP) that separates a nonmagnetic from a magnetic metallic phase [1–3]. This usually leads to the formation of new phases of matter, whose properties are dominated by quantum fluctuations. These fluctuations can be fine-tuned by an external parameter, such as chemical substitution, magnetic field or external pressure. The location and nature of QCPs are central to the understanding of the interplay between superconductivity and magnetism in these systems. In a number of heavy fermion (HF) compounds such as CePd₂Si₂, CeIn₃, and CeIrSi₃, the QCP is buried deep inside of a superconducting phase in the pressure-temperature phase diagram [2, 4, 5]. In these cases it is challenging to establish the presence of a QCP and to study the microscopic magnetic properties coexisting with superconductivity. In this μ SR study on the HF CeRhSi₃, we uncovered the previously conjectured QCP hidden inside the superconducting phase. We directly observed the disappearance of the ordered magnetic moments at the critical pressure $p^* = 23.6$ kbar deep inside the superconducting phase. This suppression of the ordered moments was found to be accompanied by a zeroing of the Néel temperature at p^* suggesting that this QCP is of magnetic nature.

CeRhSi₃ is a noncentrosymmetric HF system [6–8], suspected to display a QCP [6, 9, 10] at pressures of the order of 26 kbar. The compound features an intriguing phase diagram. It displays an AFM phase at ambient and applied pressure and a superconducting phase for pressures $p > 12$ kbar [6, 11]. Measurements of the de Haas-van Alphen effect at ambient and applied pressure show that the f -electrons are itinerant up to at

least 30 kbar [9]. Neutron diffraction at ambient pressure showed that the magnetic order is incommensurate, with ordered moments of the order of $0.1 \mu_B/\text{Ce}$ [12]. From previous results of thermal and transport properties it was established that the antiferromagnetic ordering temperature $T_N \approx 1.6$ K at ambient pressure, initially increases with increasing pressure, and then decreases towards the superconducting transition temperature $T_c \sim 1$ K for $p \approx 20$ kbar. The nature of the magnetism above this pressure across the proposed QCP inside the superconducting phase is unclear.

Single crystal CeRhSi₃ platelets were grown via a standard metal flux technique [13] with initial molar ratios of 1:1:3:30 (Ce:Rh:Si:Sn). The high quality of our single crystal samples was verified by the results of X-ray Laue diffraction and by measurements of the residual resistance ratio $\rho_{300\text{ K}}/\rho_0$ which was found to be of the order of 110.

μ SR measurements at ambient pressure were performed using the Low Temperature Facility spectrometer (LTF) at the Paul Scherrer Institut (PSI). Measurements under pressure were conducted on the General Purpose Decay-Channel spectrometer (GPD). For zero-field (ZF) and longitudinal-field (LF) measurements we typically counted 6×10^6 positron events per spectrum and 0.5×10^6 for transverse-field (TF) measurements, respectively.

The single crystal sample consisted of platelets with an average thickness of 0.1 mm. For the measurement on LTF they were attached to a silver plate, with the crystal c -axis perpendicular to the plate and parallel to the muon beam covering an area of $\sim 1 \text{ cm}^2$. For pressure-measurements they were stacked in a cylindrical volume of 1 cm^3 (mass ~ 500 mg). In addition, a 1 g polycrystalline sample of CeRhSi₃ was measured under pressure.

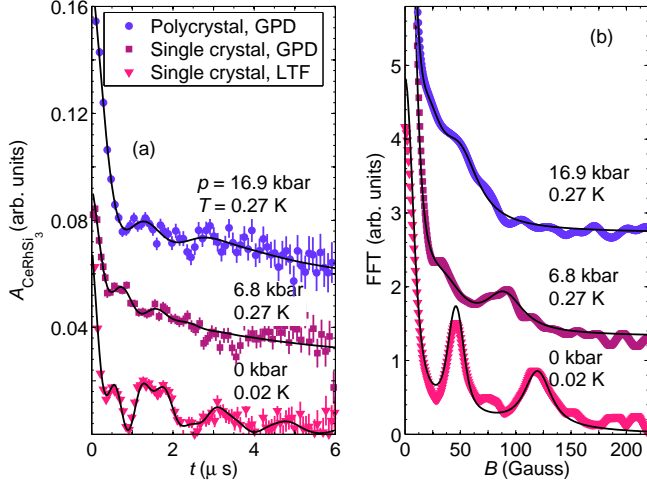


FIG. 1. (Color online) ZF measurements at various applied pressures on LTF ($p = 0$ kbar) and GPD ($p = 6.8$ and 16.9 kbar) from single crystal and polycrystalline CeRhSi_3 samples. (a) The time spectra at different pressures at base temperature (0.02 and 0.27 K, respectively) and their corresponding fits (black lines) according to Eq. (1). (b) FFTs of the time spectra shown in (a). Both the spectra in (a) and the FFTs in (b) are vertically shifted for better illustration.

In Fig. 1 ZF time spectra and the corresponding fast Fourier transforms FFTs for several pressures at a base temperature (of 0.02 K and 0.27 K for LTF and GPD, respectively), are shown for single crystal and polycrystalline samples. The signal from the Ag plate and the pressure cell, respectively, has been subtracted, (see Supplemental Material for details). The signals shown in Fig. 1 reveal a fast decay and a characteristic time structure, expected in the case of a signal containing several oscillatory components. The fast Fourier transform (FFT) of the time spectrum at $p = 0$ kbar (see Fig. 1(b)), displays three well-defined distributions of internal magnetic fields centered at $\sim 0, 45$ and 120 G. Therefore, the ZF sample asymmetry function is described here by three terms:

$$A_{\text{CeRhSi}_3}(t) = \sum_{i=1}^3 A_i \cdot g_i(t), \quad (1)$$

$$g_i(t) = \alpha \cdot \cos(\gamma_\mu B_i t) \cdot e^{-\lambda_{Ti} \cdot t} + (1 - \alpha) \cdot e^{-\lambda_L \cdot t},$$

where $\gamma_\mu/2\pi = 135.5$ MHz/T with γ_μ the muon gyro-magnetic ratio. B_i denote the average internal magnetic fields at the muon stopping sites in the sample. α was found to be $\frac{2}{3}$, which is not apriori evident for single crystals, but is always the case for polycrystalline samples. A_i are the asymmetries at time 0 of the individual components, which are proportional to the probability that a muon stops at a site with an internal field B_i . We find: $A_1 = A_2$ and $A_3 = 1.5 \cdot A_1$. λ_{Ti} and λ_L are the transverse and longitudinal muon relaxation rates, respectively. B_i , λ_{Ti} and λ_L are temperature dependent. The relations

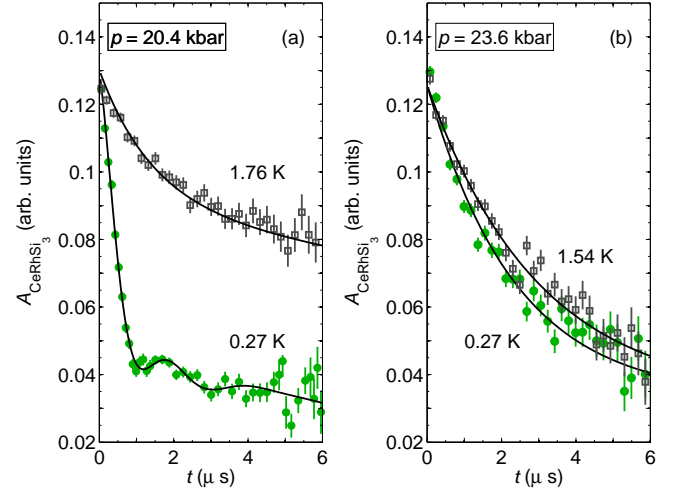


FIG. 2. (Color online) ZF data from the polycrystalline sample at (a) 20.4 kbar and (b) 23.6 kbar at two different temperatures. The time spectra were fitted using Eq. (1). The signal of the pressure cell was subtracted.

$B_1/B_2 \approx 2.6$ and $\lambda_{T1}/\lambda_{T2} \approx 2.6$ were found experimentally; B_3 was found to be roughly 0 for all temperatures and pressures.

The weights of the spectra in Fig. 1(b) shift to lower fields with increasing pressure, that is, the quasi-static internal fields are increasingly suppressed with pressure.

Since the AFM structure is incommensurate, one might expect that the quality of the fits would improve by replacing the cosine terms in Eq. (1) by Bessel functions, as in the case of UNi_2Al_3 [14, 15], CeAl_3 [15] or CeCu_5Au [16]. This replacement, however, leads to fits of lower quality, and will not be considered further here.

High-pressure data at low and high temperatures are shown in Fig. 2. In the time spectrum at 20.4 kbar and $T = 0.27$ K $\ll T_N$ we observe a fast relaxation and slow oscillations. Both of these features are absent at $T = 1.76$ K $> T_N$ showing that the low-temperature data reflects the presence of internal magnetic fields arising from magnetic order. For the data at 23.6 kbar, the fast relaxation and the oscillations are absent and there is no significant change from the high temperature to the low temperature signal at $T = 0.27$ K. This demonstrates the absence of magnetic order down to at least 0.27 K, the lowest temperature of these experiments. Since at this pressure the internal magnetic fields are zero, T_N is most likely zero.

In the results of resistivity and specific heat measurements CeRhSi_3 was found to be superconducting for $p > 12$ kbar and low T , our results therefore demonstrate that over the pressure region $12 \text{ kbar} < p < 23.6 \text{ kbar}$ superconductivity and AFM order coexist, as indicated in earlier measurements [6].

The ZF data in the AFM state shows, in addition to the tiny ordered moments, a fast initial relaxation. As

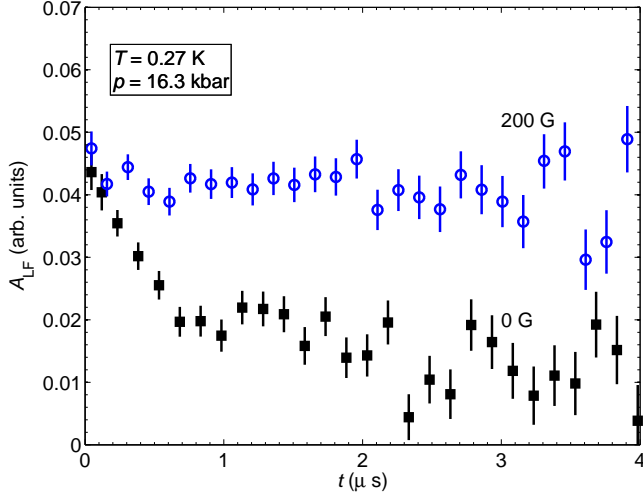


FIG. 3. (Color online) μ SR time spectra of the single crystal sample in zero and longitudinal field at $T = 0.27$ K and $p = 16.3$ kbar. The pressure cell signal (background) was subtracted.

we shall see, the fast relaxation is not caused by fluctuating (large) moments, as it would be in the case where Kondo screening were destroyed and the local Ce moments were restored. The results of μ SR measurements at longitudinal fields at $p = 16.3$ kbar (see Fig. 3) showed that at modest external fields of 200 gauss (of the order of the internal quasi-static fields) the muon relaxation is substantially suppressed; that is, magnetism is fully decoupled, which supports the quasi static origin of the relaxation at the pressure 16.3 kbar. We find no evidence for dynamical relaxation at any pressure in the low-temperature region of the AFM phase. Above T_N at $p = 0$ kbar an LF measurement was also conducted and complete decoupling was observed at an applied field of ~ 200 G. We therefore infer absence of appreciable dynamical relaxation above T_N . Thus, our data supports a scenario where the Ce moments are quenched at all pressures below p^* , and where the Kondo screening remains largely intact.

The normalized static internal fields $B_1/B_1(0)(p)$ (equivalent to $B_2/B_2(0)(p)$) extracted from the fits using Eq. (1) are depicted in Fig. 4 as a function of pressure (circles). $B_1(0)$ denotes the internal field at the lowest measured pressure $p = 0$ kbar. B_1 decreases monotonically with pressure and vanishes near $p^* \sim 23.6$ kbar, showing that magnetic order is suppressed at p^* . For the two highest measured pressures the field distribution is very broad. Still, over the entire antiferromagnetically ordered region one observes a pressure independent ratio B_1/B_2 . This implies that the magnetic structure does not change appreciably with pressure. In addition, our data show that near p^* the fast relaxation characterizing the ZF data in the AFM state vanishes.

The Néel temperature as a function of pressure was

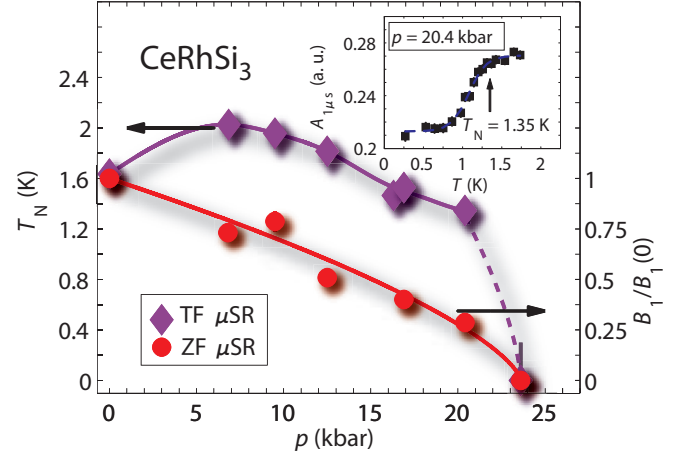


FIG. 4. (Color online) Comparison of the pressure dependence of the Néel temperature (diamonds) and the normalized internal field $B_1/B_1(0)$ (circles). The lines are guides to the eye. The inset shows the asymmetry $A_{1\mu s}$ versus temperature exemplarily for the pressure $p = 20.4$ kbar. The Néel temperature is indicated by an arrow. The dashed line is a guide to the eye.

obtained with μ SR measurements in transverse fields of 50 and 300 gauss, respectively. Below the Néel temperature the magnetic order leads to an extra fast relaxation so that the total asymmetry after some time, $t > 1\mu s$ in our case, is smaller than the corresponding amplitude above T_N . The time spectra for $t > 1\mu s$ were fitted using

$$A(t) = A_{1\mu s} \cdot \exp\left(-\frac{1}{2}(\sigma t)^2\right) \cdot \cos(\gamma_\mu B t), \quad (2)$$

where $A_{1\mu s}$ is the asymmetry at $1\mu s$ after the muon is implanted. B represents the local field and is a fit parameter. Upon cooling, one observes a rapid decrease of $A_{1\mu s}$, as the system enters the AFM state. The Néel temperature is associated with the onset of the drastic steplike reduction of $A_{1\mu s}(T)$ with decreasing temperature. One example of $A_{1\mu s}(T)$ for $p = 20.4$ kbar is shown in the inset of Fig. 4.

The results for T_N at different pressures are shown in Fig. 4 as diamonds. $T_N(p)$ shows a maximum at around 7 kbar, consistent with the results of resistivity [6, 11] and specific heat [17] measurements. By contrast, the internal fields and, therefore, the ordered magnetic moments decrease monotonically. We find that the internal fields and T_N vanish at the critical pressure of $p^* = 23.6$ kbar and magnetic order disappears. Our data show that the AFM order is completely suppressed for $p \geq p^*$, and that there is a continuous tuning of the AFM phase with pressure. All this indicates the presence of a magnetic QCP at p^* .

The different pressure dependencies of the Néel temperature and that of the internal fields may be understood using the simplified, but widely used,

one-dimensional Kondo lattice model described by S. Doniach [18]. The model considers the competing effects of the Kondo screening and the exchange interaction between Ce moments which tend to stabilize the magnetic moments leading to magnetic order. The results are summarized in the so-called Doniach phase diagram, displaying the Néel temperature T_N as a function of the product $|JN_F|$ of the exchange coupling J and the density of states of the conduction electrons at the Fermi level N_F . For low values of $|JN_F|$ the system is magnetically ordered and T_N increases with increasing $|JN_F|$. Further increase of $|JN_F|$ yields a maximum of T_N and a subsequent decrease (observed, for instance in CeAg [19]). T_N eventually reaches zero, and further increase in $|JN_F|$ yields a nonmagnetic (Fermi liquid) system.

In our case, the product $|JN_F|$ is tuned with external pressure. The observation of the maximum of $T_N(p)$ and the subsequent suppression of T_N to zero, suggests that the application of rather modest pressures leads to substantial changes of $|JN_F|$. At the same time, the Doniach model predicts a monotonic decrease of the ordered moments with increasing J according to [18] $\langle S^x \rangle = \sqrt{1 - (J/W)^2}$, where W is the conduction electron bandwidth and S^x is the x -component of a spin \mathbf{S} . These predictions match qualitatively our experimental observations.

We emphasize that the order parameter, i.e., the sublattice magnetization (or more precisely the amplitude of the spin density wave), represented here by the internal fields, displays a continuous phase transition with pressure and the Néel temperature goes to zero at p^* . This clearly reveals the presence of a QCP. In our case, it lies deep in the superconducting phase, and its bulk properties are masked by superconductivity. Nevertheless, it has been reported that between 20 – 26 kbar and $T > 1$ K, non-Fermi-liquid behavior [6] is observed in the temperature dependence of the electrical resistivity, adding support to our claim. Further indications for a QCP may be extracted from the extremely high upper critical field H_{c2} ($H_{c2} \parallel \mathbf{c}$) and its sensitivity to pressure for $p > 26$ kbar [20]. Both the behavior of the resistivity and that of H_{c2} may be explained theoretically in terms of antiferromagnetic spin fluctuations in three dimensions close to the QCP [10]. In the results of de Haas-van Alphen measurements no change in the size of the Fermi surface across p^* was observed [9]. That is, the Kondo screening of the Ce moments is active at pressures on both sides of p^* . All this hints at a *SDW* type QCP [1, 2], consistent with our findings. This type of QCP is driven by quantum fluctuations of the magnetic order parameter, as opposed to the so called *local* QCP where the Kondo screening is destroyed and the local moments are restored in the magnetically ordered phase, i.e. $p < p^*$.

In summary, we have measured the pressure evolution

of the internal fields of the AFM phase of CeRhSi₃ with the μ SR technique. As a function of pressure the internal fields diminish continuously with increasing pressure, in clear contrast to the complex behavior of the Néel temperature which shows a maximum at around 7 kbar. Our observations may be understood in the framework of the Doniach phase diagram. This analysis reveals a strong sensitivity of $|JN_F|$ to the externally applied pressure for CeRhSi₃. At $p^* \approx 23.6$ kbar the system becomes non-magnetic and signals the presence of a magnetic QCP, masked by the superconducting phase. We find no evidence for a breakdown of the Kondo screening across the QCP.

This work was performed at the Swiss Muon Source ($S\mu S$), Paul Scherrer Institut (PSI Villigen, Switzerland). Helpful discussions with A. Amato and H. Luetkens are gratefully acknowledged. We are thankful for technical support by M. Elender during the experiment. We acknowledge the financial support of the Swiss National Science Foundation. D. A. acknowledges financial support from the Romanian UEFISCDI Project PN-II-ID-PCE-2011-3-0583 (85/2011). A. D. B. received support from the Natural Sciences and Engineering Research Council of Canada (Canada), Fonds Québécois de la Recherche sur la Nature et les Technologies (Québec), and the Canada Research Chair Foundation. Work at UC Riverside was supported by U.S. NSF Grant 0801407.

Supplemental material: Background signal

In our experiments the raw μ SR signal contains two components: the signal from the sample, CeRhSi₃, and the signal from the background (bg), i.e.

$$A(t) = A_{\text{CeRhSi}_3}(t) + A_{\text{bg}}(t). \quad (3)$$

In LTF the background signal originates from muons stopped in the silver plate to which the crystals are attached, whereas in GPD the background stems from muons stopped in the pressure cell. Both cases have been extensively characterized in previous experiments and their relaxation is due to the nuclear moments of the materials. In the analysis of our data, the relaxation rates of the respective backgrounds were fixed in the fits and the only free parameter is the initial asymmetry $A_{\text{bg}}(0)$. With this restriction we perform a full fit to the data using Eq. 3, from where we extract A_{CeRhSi_3} .

The silver plate used in the LTF experiment contributes a signal that is roughly constant in the measured time window. Approximately 50% of muons stopped inside of the sample in the LTF measurements.

For the GPD measurements, we used piston-cylinder pressure cells made of CuBe ($p \leq 21$ kbar) and the Co-Ni alloy MP35 ($p > 21$ kbar), respectively [21]. The hy-

drostatic pressure was measured with an 0.1 kbar accuracy in the following way: with ac-susceptibility measurements the superconducting transition temperature T_c of an indium piece, placed inside the pressure cell, was determined. The pressure dependence of the superconducting transition of In is

$$T_c = 3.402 \text{ K} - 3.64 \cdot 10^{-2} \text{ K/kbar} \cdot p, \quad (4)$$

where p is the pressure in kbars [22].

The pressure cell contributes a rather high background compared to the signal from the sample. For the single crystal sample only 20 - 25% of the incoming muons stopped in the sample. For the polycrystalline sample the stopping fraction increased to 40%.

In zero field (ZF) the signal due to the CuBe-pressure cell can be described by a Kubo-Toyabe type polarization function [23]:

$$A_{KT}(t) = \frac{1}{3} + \frac{2}{3}(1 - (\sigma t)^2) \exp[-\frac{1}{2}(\sigma t)^2], \quad (5)$$

where σ/γ_μ is the width of the local field distribution with $\sigma = 0.33 \mu\text{s}^{-1}$ (temperature independent) for CuBe.

For the MP35-pressure cell the signal in ZF may be approximated by the product of a Kubo-Toyabe (Eq. (5)) and an exponential function, i.e. [21, 24]

$$A_{MP35(ZF)}(t) = A_{KT}(t) \cdot \exp(-\lambda t). \quad (6)$$

The relaxation rate λ is found to be temperature dependent and was fixed at each temperature to values from a calibration curve. The calibration curve was obtained at the beginning of the experiment at the measured pressure. For this purpose the energy of the incoming muons is adapted so that the muons stop only inside of the pressure cell (and not in the sample). In a weak transverse field (TF) the pressure cell is fitted by

$$A_{MP35(TF)} = A_0 \exp[-\frac{1}{2}(\sigma' t)^2] \exp(-\lambda t) \cos(\gamma_\mu B t), \quad (7)$$

with A_0 the asymmetry at time zero, $\sigma' \approx 0.33 \mu\text{s}^{-1}$ (temperature independent) and B the local field parameter. $\lambda(T)$ is marked by a strong increase below $T = 1.4 \text{ K}$. The subtraction of the MP35-pressure cell signal in the low temperature region therefore requires special care, due to its strong temperature dependence.

The signal of the (CuBe) pressure cell in a longitudinal field (LF) is described by an extended Kubo-Toyabe type function [Eq. 21 of Ref. 23 and Eq. 6.130 of Ref. 25]:

$$A_{LF}(t) = 1 - \frac{2Q'(t)}{\omega^2 t} [\cos \omega t - j_0(\omega t)] - 2 \int_0^t \frac{Q'(s)}{s} \frac{j_0'(\omega s)}{\omega} ds, \quad (8)$$

with $j_0(x) = \sin(x)/x$ and $Q(t) = \exp(-\frac{1}{2}\sigma^2 t^2)$.

* nikola.egetenmeyer@psi.ch

- [1] P. Gegenwart, Q. Si, and F. Steglich, *Nature Physics* **4**, 186 (2008).
- [2] Q. Si and F. Steglich, *Science* **329**, 1161 (2010).
- [3] P. Coleman and J. Schofield, *Nature* **433**, 226 (2005).
- [4] N. D. Mathur, *et al.*, *Nature* **394**, 39 (1998).
- [5] R. Settai, *et al.*, *J. Phys. Soc. Jpn.* **77**, 073705 (2008).
- [6] N. Kimura, Y. Muro, and H. Aoki, *J. Phys. Soc. Jpn.* **76**, 051010 (2007).
- [7] Y. Muro, D. Eom, N. Takeda, and M. Ishikawa, *J. Phys. Soc. Jpn.* **67**, 3601 (1998).
- [8] Y. Muro, *et al.*, *J. Phys. Soc. Jpn.* **76**, 033706 (2007).
- [9] T. Terashima, *et al.*, *Phys. Rev. B* **76**, 054506 (2007).
- [10] Y. Tada, N. Kawakami, and S. Fujimoto, *Phys. Rev. B* **81**, 104506 (2010).
- [11] N. Kimura, *et al.*, *Phys. Rev. Lett.* **95**, 247004 (2005).
- [12] N. Aso, *et al.*, *J. Mag. Mag. Mat.* **310**, 602 (2007).
- [13] P. C. Canfield and Z. Fisk, *Philosophical Magazine Part B* **65**, 1117 (1992).
- [14] Y. J. Uemura and G. M. Luke, *Physica B* **186-188**, 223 (1993).
- [15] A. Amato, *Rev. Mod. Phys.* **69**, 1119 (1997).
- [16] A. Amato, *et al.*, *Phys. Rev. B* **52**, 54 (1995).
- [17] F. Tomioka, *et al.*, *J. Mag. Mag. Mat.* **310**, 340 (2007).
- [18] S. Doniach, *Physica B* **91**, 231 (1977).
- [19] A. Eiling and J. S. Schilling, *Phys. Rev. Lett.* **46**, 364 (1981).
- [20] N. Kimura, K. Ito, H. Aoki, S. Uji, and T. Terashima, *Phys. Rev. Lett.* **98**, 197001 (2007).
- [21] D. Andreica, Ph.D. thesis, IPP/ETH-Zurich (2001).
- [22] A. Maisuradze, A. Shengelaya, A. Amato, E. Pomjakushina, and H. Keller, *Phys. Rev. B* **84**, 184523 (2011).
- [23] R. Kubo, *Hyperfine Interact.* **8**, 731 (1981).
- [24] R. Khasanov, *et al.*, e-print: arXiv: **0908.2734v1** (2009).
- [25] A. Yaouanc and P. Dalmas de Réotier, *Muon Spin Rotation, Relaxation, and Resonance*, edited by J. Birman, S. F. Edwards, R. Freind, M. Rees, D. Sherrington, G. Veneziano (Oxford University Press, 2011).